842

2.B:2.L

Nuclear Physics A350 (1980) 345–364

DOUBLE CHARGE EXCHANGE AND ONE-PION PRODUCTION IN π^+ ^{4}He COLLISIONS AT 1.7 GeV/c*

J.-B. JEANNERET**, M. BOGDANSKI*** and E. JEANNET

*Institute of Physics of the University of Neuchâtel****, Rue A.-L. Breguet 1, CH-2000 Neuchâtel, Switzerland*

Received 5 June 1980

Abstract: We present the results of a study of the exclusive reactions π^+ ^{4}He $\rightarrow \pi^-$ 4p (double charge exchange, DCE) and π^+ ^{4}He $\rightarrow \pi^+\pi^-$ 3pn (one-pion production). The experiment was performed with the Oxford/RHEL helium bubble chamber irradiated with a 1.7 GeV/c π^+ beam. A general review of DCE models is presented and experimental results at other energies are discussed in the light of these models. None of the existing theoretical models is compatible with out data at 1.7 GeV/c. We propose a new mechanism for DCE, involving three nucleons, which reproduces the integrated as well as the differential cross sections. Some consequences for other models are also discussed.

E NUCLEAR REACTIONS $\alpha(\pi^+, \pi^-)$, $(\pi^+, \pi^+\pi^-)$, E = 1.71 GeV: measured σ, $\sigma(0)$. Discussed reaction mechanism.

1. Introduction

The double charge exchange of a pion on a nucleus is of great interest in the study of nuclear mechanisms. In principle, it allows one to study the correlations between nucleons inside the nuclei, and it is the only reaction directly exhibiting double scattering mechanisms in the ^{4}He nucleus. Due to its relative simplicity, the ^{4}He nucleus has been extensively studied. Various mechanisms have been proposed for the DCE type of reaction, but due to the lack of experimental data, they have not yet been tested.

This work is a continuation of our bubble chamber study of double charge exchange on ^{4}He between 1.5 and 2.0 GeV/c [ref. [21])]. We present here the final results obtained at 1.7 GeV/c.

This paper is structured in the following way. In sect. 2 we describe the experimental method and give the values obtained for the integrated cross sections. In sect. 3 we present results and a discussion of the reaction π^+ ^{4}He $\rightarrow \pi^+\pi^-$ 3pn. In sect. 4,

* The present paper summarizes the Ph.D. thesis of one of the authors (J.-B.J., University of Neuchâtel).

** Now at CERN Geneva, Switzerland.

*** Now at the Laboratoire Suisse de Recherches Horlogères, Neuchâtel, Switzerland.

**** Work also supported by the Swiss National Science Foundation.

which is devoted to the $\pi^+ {}^4\mathrm{He} \to \pi^- 4\mathrm{p}$ reaction, we discuss different double charge exchange models in the light of our results.

2. Experiment

2.1. THE BUBBLE CHAMBER

The Oxford/RHEL helium bubble chamber [3]) had a useful volume of $88.5 \times 44.0 \times 47.5$ cm^3. The liquid helium was at a temperature of 3 K and at a pressure of 0.3 atm [ref. [4])]; its density was obtained by measuring the range of μ^+ produced by the decay of stopping π^+ inside the chamber and by integrating the Bethe–Bloch relation for $(\mathrm{d}E/\mathrm{d}x)$ [ref. [5])], where the density was left undefined. We obtained the value $\rho = 0.140 \pm 0.007$ g/cm^3.

The magnetic field had a nominal value of $B_z^0 = 21.024$ kG in the centre of the chamber, and the three field components over the entire volume were given by a three-dimensional field map.

2.2. THE BEAM

For this experiment the helium bubble chamber was exposed to the BM3 beam of the Nimrod accelerator. Separation of protons and pions was achieved by an electrostatic separator [4]). The contamination due to positrons was compatible with zero [4]), and was small for K^+ (0.5‰) and for μ^+ (5‰) [ref. [1])].

The nominal beam momentum depended on the scanning criteria due to a small correlation with the incident angle at the entry of the chamber. The mean value adopted, $p = 1.71 \pm 0.12$ GeV/c, was defined by the incident incoming pions of all the events retained.

2.3. SCANNING AND MEASURING

Seventeen thousand pictures were scanned. Among them twelve thousand were scanned twice in order to calculate the scanning efficiency. For the evaluation of absolute cross sections, beam tracks were counted every fifty frames.

The two reactions of interest exhibit the same topology: one negative and four positive tracks, the latter often being very short (a proton of momentum $p =$ 100 MeV/c has a range of 2.8 mm in liquid helium).

Events selected at the scanning stage were measured on a semi-automatic device, ENETRA. Before measurement, each event was again observed in the four available views, in order to check the topology. Each vertex was examined carefully to determine whether very short stopping tracks could be parasitic bubble clusters of δ-rays. Events not passing this test were classified as topological rejects and eliminated from all further efficiency calculations. The measurement was then done

on the three best views. The momenta of stopping tracks were calculated using the range-energy relations, whereas the momentum of a track leaving the chamber was calculated by using the curvature – defined by the measured points – and the magnetic field.

The geometrical and kinematical reconstruction was done with the CERN programs THRESH [7]) and GRIND [7]) respectively. The precision obtained for the measurements was:

$$\pi^+ \text{ (beam)}: \sim 50\ \text{MeV}/c, \qquad \pi^{\pm} \text{ (outgoing)}: \sim 25\ \text{MeV}/c,$$

$$\text{protons}: \sim 35\ \text{MeV}/c, \qquad \text{stopping protons}: \sim 7\ \text{MeV}/c.$$

2.4. SEPARATION OF HYPOTHESES

For each measured event kinematical fits were made to the four following hypotheses:

$$\pi^+ {}^4\text{He} \rightarrow \pi^+ \pi^- 4\text{p (i)}, \qquad \pi^+ {}^4\text{He} \rightarrow \pi^+ 4\text{p}\pi^0 \text{ (ii)},$$

$$\pi^+ {}^4\text{He} \rightarrow \pi^+ \pi^- 3\text{pn (iii)}, \qquad \pi^+ {}^4\text{He} \rightarrow \pi^+ \pi^- 2\text{pd (iv)}.$$

Fits (i) and (iv) give four-constraint fits, while (ii) and (iii) are one-constraint. Ambiguities were resolved by comparing the bubble density computed by GRIND for each track with the density visually observed on the frame. There were no ambiguities between reaction (i) and any of the others. In reaction (iii) there were 50 ambiguous events out of 1500 due to the possible interchange of the π^+ with a proton. The ambiguities usually occurred when a track was measured only over a short distance (≤ 5 cm) due to a secondary interaction. Those events were considered to be measured rejects.

The separation of reactions (iii) and (iv), however, was more difficult: there was an overlap of 90% in the samples of these two reactions. This is due to the very small binding energy of the deuteron compared to the experimental energy resolution. In addition, for a slow particle it is impossible to distinguish a proton from a deuteron, since the bubble density reaches saturation. The following consideration resolved the problem: since reaction (iv) represents a 4C-fit, a type (iii)–(iv) ambiguous event was considered as belonging to category (iv) only in the case of perfect collinearity between a proton and the neutron. Hence, reaction (iv) may contaminate reaction (iii) but not vice-versa. In fig. 1 are shown the neutron momentum distributions corresponding to events retained after measurement:

(a) under hypothesis (iii) only,

(b) under hypotheses (iii) and (iv).

The deuteron distribution of sample (iv) [ref. [8])] enables one to calculate the missing momentum distribution assigned to the neutron (distribution c, fig. 1). The similarity of distributions b and c, both clearly different from a, establishes the excellent separation of reactions (iii) and (iv).

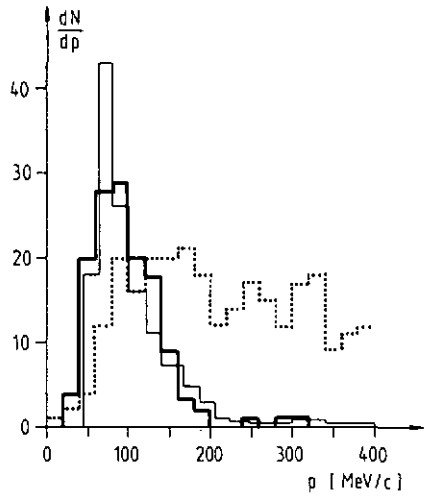

Fig. 1. Neutron momentum distribution: dotted line events of type (a) (see text); heavy line events of type (b); light line calculation for events of type (b).

In figs. 2a and 3a are shown the missing mass distribution of reactions (i) and (iii) obtained after a χ^2 probability cut at 40% for reaction (i) and at 6% for reaction (iii)

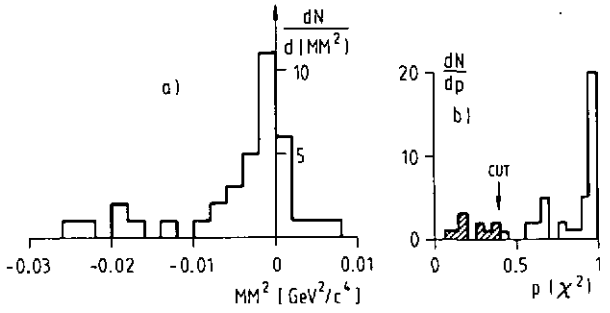

Fig. 2. Double charge exchange [reaction (i)]: (a) missing mass-squared distribution, (b) χ^2 probability distribution. The χ^2 probability distribution is not flat because the error of the missing mass is not gaussian for 4C-fit events [9]. This explains the asymmetry of the missing mass distribution, and also the high probability cut ($p_{cut} = 40\%$) made in order to eliminate the contamination.

(figs. 2b and 3b). Thus, the contamination from low-probability events was eliminated. A weak resolution is found in the neutron mass distribution (MM). This is due to an increasing dependence of the error σ on MM^2 [refs. [7,9])]. It has been previously demonstrated that the sample is not contaminated by events containing an additional π^0 [ref. [1])].

The numbers of events used are given in table 1. The analysis of reaction (iv) has been presented in a separate publication [8]).

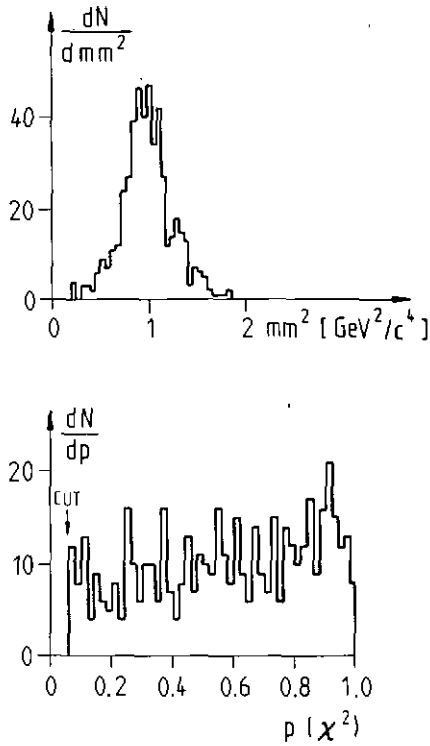

Fig. 3. One-pion production [reaction (iii)]: (a) missing mass-squared distribution, (b) χ^2 probability distribution.

TABLE 1

Cross sections

Reaction	No events	σ^u (mb)	σ (mb)
$\pi^+ {}^4\mathrm{He} \to 4\,\mathrm{pos} + 1\,\mathrm{neg}$	1506	11.2 ± 0.7	
$\pi^+ {}^4\mathrm{He} \to 3\,\mathrm{pos} + 1\,\mathrm{neg}$	174	3.1 ± 0.3	
$\pi^+ {}^4\mathrm{He} \to \pi^+\pi^- 3\mathrm{pn}$	487	3.73 ± 0.25	3.07 ± 0.22
$\pi^+ {}^4\mathrm{He} \to \pi^+\pi^- 2\mathrm{pd}$	129		1.22 ± 0.16 [a]
$\pi^+ {}^4\mathrm{He} \to \pi^+\pi^- \mathrm{p}\,{}^3\mathrm{He}$	26 ± 7 [b]		4.3 ± 1.3 [b]
$\pi^+ {}^4\mathrm{He} \to \pi^- 4\mathrm{p}$	39	0.24 ± 0.04	0.25 ± 0.05

[a]) Ref. [8]).
[b]) See text.

2.5. CROSS SECTIONS

The uncorrected cross sections were obtained by the formula

$$\sigma_r^u = \frac{1}{n_0 L} \frac{N_r}{\varepsilon_{sc}\varepsilon_{mes}},$$

where n_0 is the number of atoms per cm^3 in liquid helium: $(2.11 \pm 0.11) \times 10^{22}$ cm^{-3}, L is the total length of incident tracks, ε_{sc} is the scanning efficiency: 0.998 ± 0.001, ε_{mes} is the measuring and processing efficiency: 0.651 ± 0.026 (this rather low value was due to the poor quality of part of the film) and N_r is the number of events found for channel r. The results for σ_r^u are given in table 1.

As seen in fig. 4 the proton momentum distribution for reaction (iii) shows a strong accumulation of events at low momentum due to the presence of spectator protons in

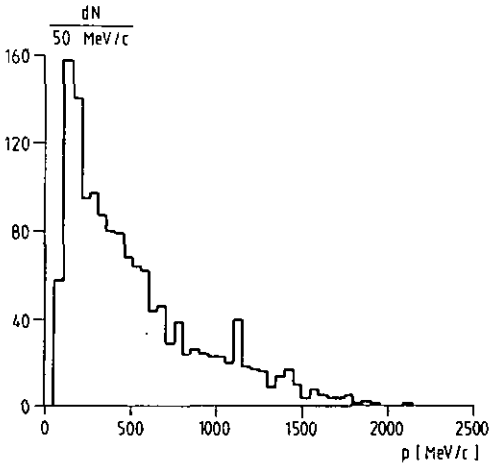

Fig. 4. Proton momentum distribution for reaction (iii). Momenta of all three protons of each event are shown.

this reaction. Fig. 5 shows the proton range, projected in the plane of the cameras. There one observes a clear cut at 1 mm: events with a track shorter than 1 mm were either not observed during scanning or rejected by the program GRIND because of high angular inaccuracy for short-range tracks.

The motion of the nucleons inside the ^{4}He nucleus can be well described by a harmonic oscillator model [10,11]). Using the impulse approximation one can

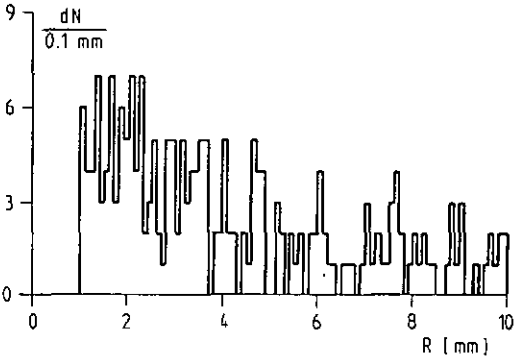

Fig. 5. Projected range of protons into the camera plane for reaction (iii).

reproduce the momentum distribution of the spectator protons with a function of the type $g(p) = A^2 \exp(-\alpha p^2)$, corresponding to the harmonic oscillator ground state (1S). The standard value assumed for α is $(\frac{1}{125}\,\mathrm{MeV}/c)^2$ [ref. [12])].

For reaction (iii) the number of spectator protons was determined by using the momentum distribution of the proton in each event with the lowest momentum in the laboratory system. Furthermore, it was required that $\theta_{lab} > 90°$. This was done in order to lower the number of protons participating in the reaction (reaction protons) which are preferentially emitted in the forward direction (fig. 6). The procedure was

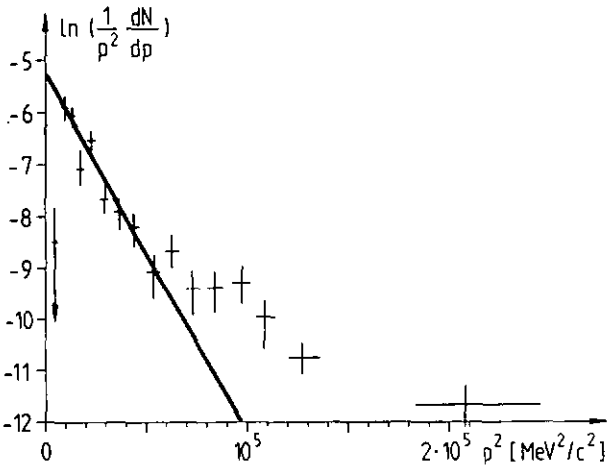

Fig. 6. Momentum distribution for slowest proton with the condition $\cos\theta < 0$. The square of the harmonic oscillator wave function is represented by the straight line (see text).

repeated using the momentum distribution of protons with low and medium momentum as well (fig. 7), since this reaction may yield events having two spectator protons.

A least-squares fit was made to the data in the momentum region $10^4 < p^2 < 7\times10^4\,(\mathrm{MeV}/c)^2$ (symmetrical errors assumed). With these fitted parameters the constraints A and α of $g(p)$ were calculated. By integrating $g(p)$ one may obtain an estimate for the number N_1 of events containing at least one observed spectator proton (see table 2).

In fig. 7 a background due to reaction protons is evident and this contribution must be subtracted. The linear behavior of this background was fitted by a straight line (d_2) through the points with $p^2 > 9\times10^4\,(\mathrm{MeV}/c)^2$, and was extrapolated to smaller p^2. Subtracting d_2 from points below $p^2 = 9\times10^4\,(\mathrm{MeV}/c)^2$ resulted in another set of points to which a new straight line (d_1) was fit, corresponding to the spectator proton spectrum. Thus, the total number N_s of observed spectator protons may be derived from the fit parameters. The difference $N_2 = N_S - N_1$ (see table 2) shows no indication of the presence of events with two spectator protons.

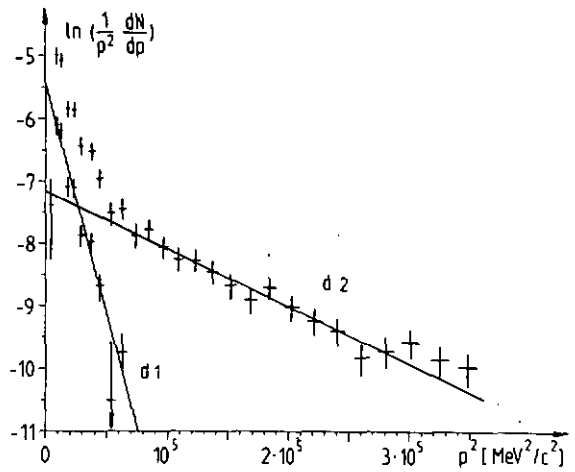

Fig. 7. Momentum distribution for slowest and medium protons (see text and comment in fig. 6). The subtracted data and d_1 are shifted down by one unit.

TABLE 2

Reaction $\pi^+ {}^4\text{He} \to \pi^+\pi^- 3\text{pn}$

	Uncorrected	Corrected
events	$N = 487$	$N_c = 578 \pm 8$
events with 0 p_s	$N_0 = 173 \pm 32$	$N_{0c} = 178 \pm 32$
events with 1 p_s	$N_1 = 314 \pm 32$	$N_{1c} = 400 \pm 30$
events with 2 p_s	$N_2 = -7 \pm 10$	—
total number of p_s	$N_s = 307 \pm 22$	$N_{sc} = 386 \pm 26$

The fraction of non-observed protons (see table 2) was calculated for spectator protons by integrating the product of $g(p)$ and the probability for the non-observance of the proton of momentum p. This probability is given by the aperture in which the proton has a projected range lower than 1 mm. An isotropic distribution for spectators was assumed.

For the reaction protons, the function corresponding to the straight line d_2 (see fig. 7) was substituted for $g(p)$, and the calculation was performed in the same manner. The corrected event number was obtained by separately correcting the values N_0 and N_1 (see table 2).

The method used for the double charge exchange reaction (i) was similar to that used for (iii). Table 3 gives a summary of the results. The cross sections were corrected for the loss of slow protons by multiplying the raw results by the ratio N_c/N (see tables 2 and 3). They were also corrected to take into account the χ^2 probability cut (see subsect. 2.4).

Complementary to one-pion production (iii) and (iv) with a 5-prong topology, 4-prong events (one negative and three positive tracks) were also studied, in order to

TABLE 3

Reaction $\pi^+ {}^4\mathrm{He} \to \pi^- 4\mathrm{p}$

	Uncorrected	Corrected
events	$N = 39$	$N_c = 46 \pm 9$
events with 0 p_s	$N_0 = 14 \pm 6$	$N_{0c} = 14 \pm 6$
events with 1 p_s	$N_1 = 25 \pm 6$	$N_{1c} = 32 \pm 8$

isolate events of the type $\pi^+ {}^4\mathrm{He} \to \pi^+ \pi^- \mathrm{p}\ {}^3\mathrm{He}$. Only a rough estimate of the integrated cross section may be given for this reaction. This value was obtained by making subtractions to the topological cross section. Further details on the calculation are given in ref. [2]). The value given in table 1 has been corrected for the loss of events where the ^{3}He recoil is not visible. The momentum distribution for ^{3}He is assumed to be the same as that for the neutron which interacts with the incident pion.

3. One-pion production

3.1. CROSS SECTIONS

The cross sections (σ^u and σ) for the three one-pion production channels are given in table 1. Their total $\sigma_1 = 8.6 \pm 1.3$ mb may be compared to [13,14]):

$$\sigma_2 = 2\sigma(\pi^+ \mathrm{n}_{\mathrm{free}} \to \pi^+ \pi^- \mathrm{p}) = 14.5 \pm 1.0 \text{ mb}.$$

The difference $\sigma_2 - \sigma_1 = 5.9$ mb may be explained by the screening effect of 3 nucleons and inelastic interactions in the final state (e.g. $\pi^- \mathrm{p} \to \pi^0 \mathrm{n}$, see also sect. 4).

3.2. THE REACTION $\pi^+ {}^4\mathrm{He} \to \pi^+ \pi^- 3\mathrm{pn}$

Fig. 8 shows the neutron momentum distribution for this reaction. The fit of two straight lines to this distribution gives evidence of a strong similarity between the behavior of neutrons and that of protons (fig. 6). In particular, the proportion of spectator neutrons is the same as that of protons (table 4). The similarity of the two distributions is illustrated by fig. 9.

Using the parameters for $d_1(p)$ of fig. 6 and the formalism of the harmonic oscillator model applied to the ^{4}He nucleus [12,15]), the rms $\langle r^2 \rangle$ of ^{4}He for protons was calculated. Applying the formula $\langle r^2 \rangle_{\mathrm{ch}} = \langle r^2 \rangle + \langle r_{\mathrm{p}}^2 \rangle_{\mathrm{ch}}$ with $\langle r_{\mathrm{p}}^2 \rangle^{1/2} = 0.8$ fm [12]) one obtains:

$$\langle \mathrm{r}^2 \rangle_{\mathrm{ch}}^{1/2} = 1.74 \pm 0.08 \text{ fm}.$$

This result is compatible with the value obtained by Plattner and Sick [16]), who combined electron scattering results and measurements done on muonic atoms:

$$\langle r^2 \rangle_{\mathrm{ch}}^{1/2} = 1.6726 \pm 0.0076 \text{ fm}.$$

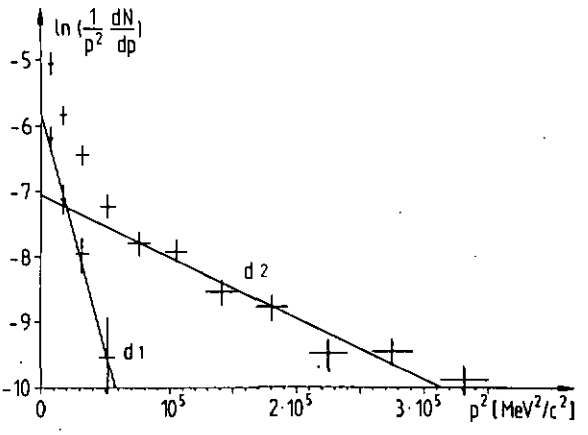

Fig. 8. Neutron momentum distribution (see text and comment in figs. 6 and 7).

TABLE 4

Comparison between $\pi^+ {}^4He \to \pi^+\pi^-3pn$ and $\pi^+ d \to \pi^+\pi^- pp$ reactions

	$\pi^+ {}^4He \to \pi^+\pi^-3pn$		$\pi^+ d \to \pi^+\pi^- pp$ [13])	
fraction of spectator nucleons	protons 0.22 ± 0.02	neutrons 0.18 ± 0.03	0.85	
pion distributions	looks like phase space distributions for $\pi^+\pi^-2pnp_s$ final state		strongly forward peaked	
resonance yields	ρ^0:	$(3 \pm 1.5)\%$	ρ^0:	$(65 \pm 6)\%$ $(61 \pm 3)\%$ [a])
	Δ^{++}:	$(16 \pm 8)\%$	Δ^{++}:	$(5 \pm 1)\%$ $(6 \pm 2)\%$ [a])
	N^{*0}:	$(10 \pm 4)\%$	N^{*0}:	—

[a]) These values correspond to $p_{beam} = 1.53$ GeV/c, which is at the same c.m. energy as $p_{beam} = 1.7$ GeV/c, but taking into account the fact that the interacting neutron is off-shell by 60 MeV/c^2, when the other nucleons are spectators.

The pion momentum distribution (fig. 10) indicates that the reaction is of the type $\pi^+ {}^4He \to \pi^+\pi^- 2pnp_s$ rather than $\pi^+ {}^4He \to \pi^+\pi^- p2p_sn_s$ (p_s and n_s denote spectator nucleons). This is confirmed by the small number of spectator nucleons (table 4) and by the similarity of the momentum distributions for protons and for neutrons.

Fig. 11 shows a very small signal of the ρ^0 resonance in the $\pi^+\pi^-$ mass distribution, in contrast to what is observed in the basic process $\pi^+ n \to \pi^+\pi^- p$ (table 4). The ρ^0 production-rate (table 4) is estimated by the shadowed region of fig. 11. The weakness of the signal does not merit the application of more sophisticated techniques.

In order to investigate the possibility of baryonic resonance the $\pi^- p$ mass spectrum was subtracted from the $\pi^+ p$ mass spectrum $(dN(\pi^- p)/dm$ and

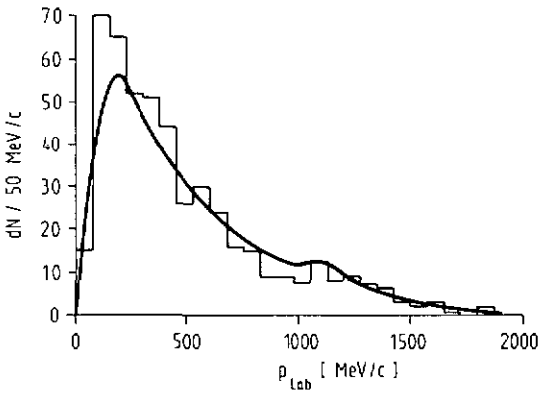

Fig. 9. Neutron momentum distribution. The continuous curve represents the proton momentum distribution convoluted with a gaussian function ($\sigma = 75$ MeV/c) representing the momentum resolution for neutrons (≡ missing momentum of the events).

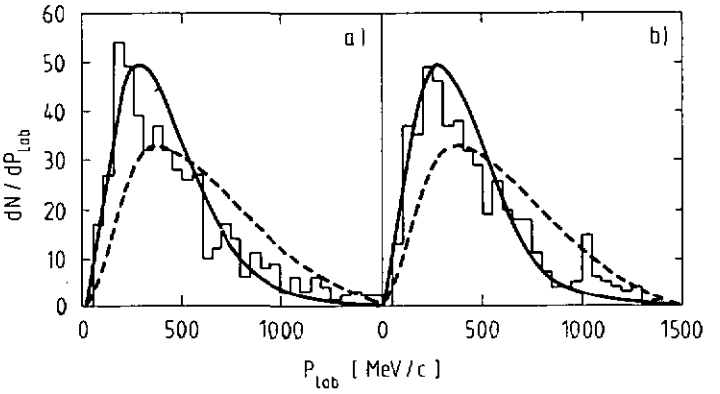

Fig. 10. Pion momentum distributions: (a) π^+, (b) π^-. The continuous curve represents the Lorentz-invariant phase space (LIPS) for the reaction $\pi^+ {}^4\mathrm{He} \to \pi^+\pi^- 2\mathrm{pnp_s}$. The dashed curve represents the LIPS for the reaction $\pi^+ {}^4\mathrm{He} \to \pi^+\pi^- \mathrm{p2p_sn_s}$. These phase space curves were calculated using the FOWL program [17]).

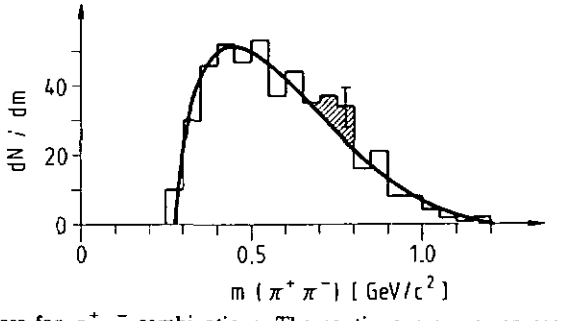

Fig. 11. Invariant mass for $\pi^+\pi^-$ combinations. The continuous curve represents the LIPS for the reaction $\pi^+ {}^4\mathrm{He} \to \pi^+\pi^- 2\mathrm{pnp_s}$.

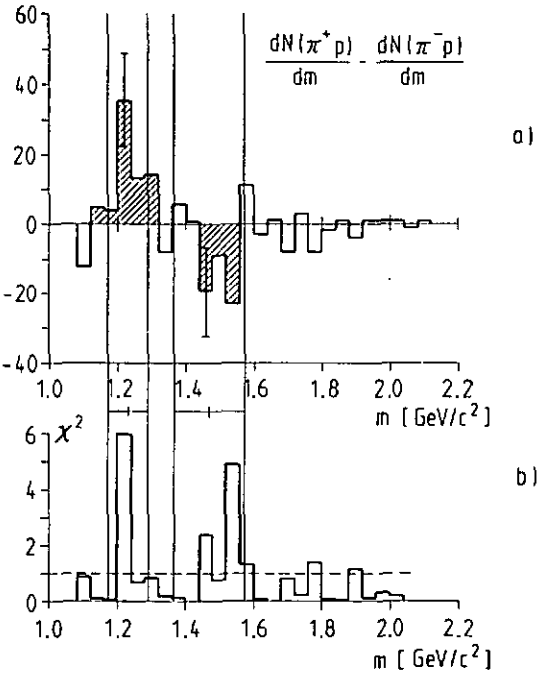

Fig. 12. (a) Difference of the mass spectra π^+p and π^-p (all combinations). (b) χ^2 distribution for each bin of (a) compared to zero.

$dN(\pi^+p)/dm$ on fig. 12), and similarly for the π^+n and the π^-n mass spectrum. This process eliminates the parasitic component due to spectator nucleons which are not separable individually from the reaction nucleons. If one assumes that the overlapping of isospin $I = \frac{1}{2}$ and $\frac{3}{2}$ is small in the region $m < 2$ GeV/c^2 (which is sufficient within the limits of our statistical precision), then the result of the subtraction is given by:

$$\frac{d(N(\pi^+p) - N(\pi^-p))}{dm} = \frac{8}{9}|\langle T_{3/2}\rangle|^2\phi - \frac{4}{9}|\langle T_{1/2}\rangle|^2\phi\,,$$

where ϕ is the Lorentz-invariant phase space factor and $\langle T_{3/2}\rangle$ and $\langle T_{1/2}\rangle$ represent the resonances $\Delta(1232)$ and N*(1470) respectively. Under the hypothesis of non-overlapping of the amplitudes, the contributions of $\langle T_{1/2}\rangle^2$ and $\langle T_{3/2}\rangle^2$ are given by the shadowed regions of fig. 12 for the spectrum $\pi^+p - \pi^-p$. In the case of π^-n and π^+n the number of events is too small to manifest any significant signals. The production rates of the different resonances observed are given in table 4.

Also shown in table 4 are the characteristics of pion production in the reaction $\pi^+d \to \pi^+\pi^-$ pp [ref. [13])]. Due to the low binding energy and the large radius of the deuteron, this reaction is similar to pion production on free neutrons. The comparison between the two reactions shows a very strong attenuation of the ρ^0

signal and larger production of baryonic resonances, as well as the presence of very few spectator nucleons in the ^{4}He case. These differences suggest a strong πN final-state interaction. This hypothesis is strengthened by the observation mentioned above, i.e. the identical behavior of protons and neutrons on the one hand (which would not be the case for $\pi^+ {}^4\text{He} \to \pi^+\pi^- \text{p2p}_s\text{n}_s$) and of positive and negative pions on the other hand. Hence, it seems – when this reaction leaves three spectator nucleons – that the production of ^{3}He is strongly favored with respect to the production of three free nucleons. This implies a very strong overlapping of the nucleon wave functions in ^{3}He and ^{4}He.

4. Double charge exchange (DCE) on ^{4}He

4.1. CROSS SECTIONS

A summary of cross section measurements for the DCE reaction $\pi^+ {}^4\text{He} \to \pi^- 4\text{p}$ is given in table 5 and fig. 13. The results at 142 MeV/c [ref. [18]), 610 MeV/c [ref. [20]) and above 1 GeV/c [ref. [21]) and this work] come from bubble chamber experiments, whereas the measurements done between 190 and 260 MeV/c [ref. [19])] used a streamer chamber. Two partial cross-section measurements from the reaction $\pi^- {}^4\text{He} \to \pi^+ 4\text{n}$ complete the integrated cross section measurements [22,23]). In one of the experiments [22]) the incident beam momentum was varied between 310 and 390 MeV/c. In the other case [23]) it was fixed at 240 MeV/c. Gibbs [24]) noted a very large incompatibility between the measurements done by Kaufman *et al.* [23]) and those done by Falomkin *et al.* [19]).

TABLE 5

Integrated cross sections for the reaction $\pi^+ {}^4\text{He} \to \pi^- 4\text{p}$

p_{lab} (MeV/c)	T_{lab} (MeV)	σ (mb)	Ref.
142	60	$(2^{+2}_{-1})\,10^{-3}$	[18])
192	98	0.30 ± 0.10	[19])
236	135	0.29 ± 0.11	[19])
248	145	0.34 ± 0.17	[19])
260	156	0.13 ± 0.07	[19])
610	486	1.20 ± 0.21	[20])
1460 ± 120	1327	0.41 ± 0.14	[21])
1710 ± 110	1576	0.25 ± 0.05	This work
1860 ± 130	1725	0.14 ± 0.07	[21])

4.2. MODELS

Predictions for the integrated cross sections of DCE on ^{4}He are presented in fig. 13. They may be classified as either pair correlation models or models based on exchange currents.

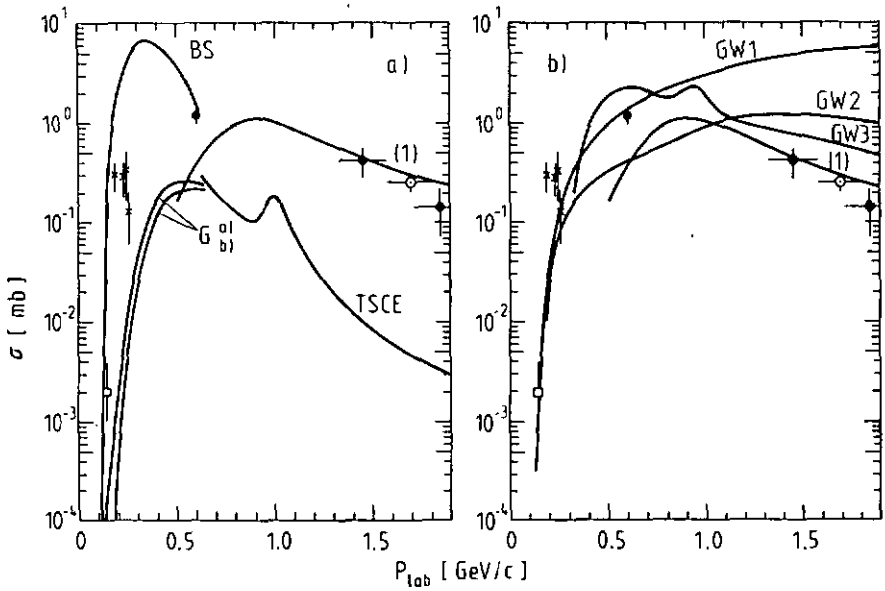

Fig. 13. Integrated cross sections for the double charge exchange reaction (DCE) π^+ ^{4}He $\rightarrow \pi^-$4p. References for experimental results may be found in table 5. Notations for models: BS, Becker and Schmit; G: Gibbs *et al.*, curve (a) without applying Pauli principle to final state protons, (b) applying Pauli principle; TSCE: two successive single charge exchanges, classical estimation; GW1–3, Germond and Wilkin; (1): present model, see subsect. 4.4. See text for references.

4.2.1. Pair correlation models. These models use two single successive charge exchanges correlated by an intermediate off-shell pion, as shown in fig. 14a. The models of Becker and Schmit [25]) (BS) and, more recently, of Gibbs *et al.* [24]) (G) essentially differ in the off-shell extension adopted for πN scattering. The large difference between the two predictions shows the extreme sensitivity of DCE to off-shell effects at low energy. Neither of the two models correctly reproduces all data: the BS model overestimates the low-energy cross section, whereas the G model correctly reproduces the data of Kaufman [23]) and Gilly [22]), but cannot explain the measurement at 600 MeV/c [ref. [20])]. The remark by Gibbs [24]) (see subsect. 4.1) clearly shows the necessity of new measurements below 500 MeV/*c*. The simplest estimate of the TSCE (two single charge exchange) model uses the formula

$$\sigma(\pi^+ \rightarrow \pi^-) = 2\sigma(\pi^+ n \rightarrow \pi^0 p)\sigma(\pi^0 n \rightarrow \pi^- p)\langle 1/4\pi r^2 \rangle ,$$

where r is the distance between the neutrons of ^{4}He. At 1.7 GeV/c this model predicts a cross section which is fifty times smaller than the measured value. Hence, another mechanism is necessary to explain DCE at high energies.

4.2.2. Models based on exchange currents. The basic idea underlying the model developed by Germond and Wilkin [27,28]) is the following: the incident pion is scattered by an off-shell pion which is exchanged between the nucleons in the nucleus (fig. 14b). Using the Weinberg model for $\pi\pi$ scattering [27]) they obtain the curve GW1 (fig. 13b). The curve marked GW2 results from using the Veneziano model

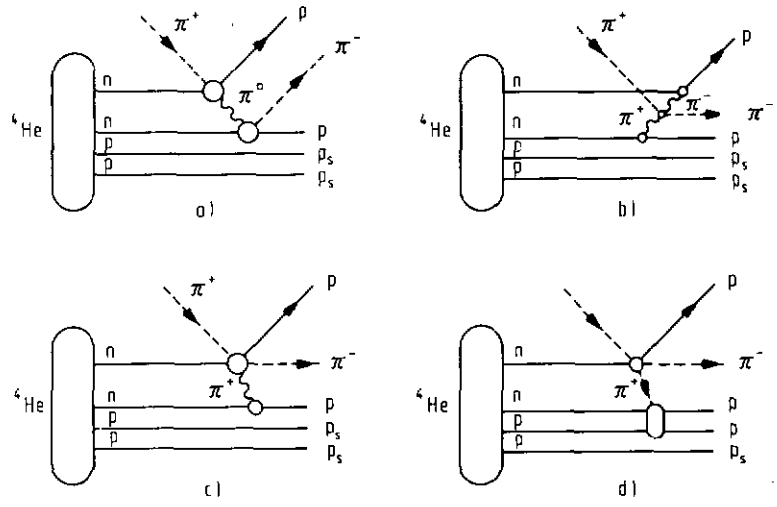

Fig. 14. Diagrams corresponding to models: (a) two single charge exchanges (TSCE, BS, G), (b) exchange currents (GW1, GW2), (c) off-shell π^+ production and absorption (GW3), (d) on-shell π^+ production and absorption on a proton–neutron pair.

modified by Lovelace [28]). The curve marked GW3 was obtained [28]) by contracting the two upper vertices of fig. 14b, which leads to an evaluation of the fig. 14c. These models reproduce perfectly the cross section below 600 MeV/c. The GW1 [27]) model correctly reproduces the differential spectra at 600 MeV/c [ref. [20])], except for the π^- forward angles region, which is overestimated. However, the models clearly overestimate the cross section above 1 GeV/c. Only the GW3 model gives the right order of magnitude at high energies. The authors [28]) do not indicate the differential cross sections for this experiment [this work and ref. [21])].

4.3. DIFFERENTIAL CROSS SECTIONS AT 1.7 GeV/c

The differential cross sections in function of momenta, polar angles and invariant masses are given in figs 15 to 18. The proton spectra only contain data for the three fastest protons of each event, the slowest proton being a spectator 70% of the time (see table 3).

The dashed curves shown in the figures correspond to the Lorentz-invariant phase space calculated for the reaction $\pi^+ + (3N)^{+1} \rightarrow \pi^- 3p$, neglecting the Fermi motion of the spectator proton. The mass used for the (3N) system was the ^{4}He mass, less the mass and mean kinetic energy of a spectator proton.

The experimental distributions which deviate the most from phase space are the following:

(i) the π^- distributions, which are peaked slightly forward and

(ii) the proton–proton invariant mass distribution, which exhibits large bump between 2.0 and 2.2 GeV/c^2.

The continuous curves are explained in the next subsection.

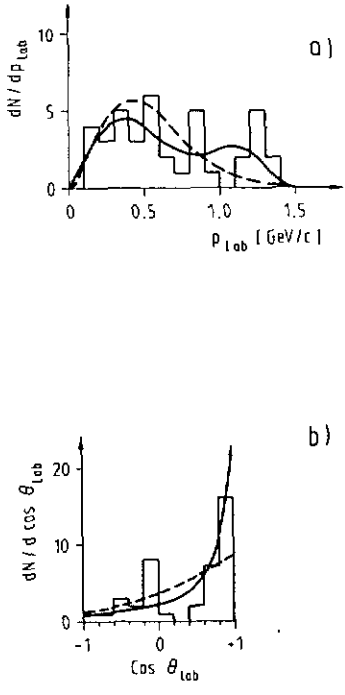

Fig. 15. DCE reaction: (a) π^- momentum distribution, (b) π^- angular distribution. The continuous curve corresponds to the model described in the text, while the dotted curve corresponds to the LIPS.

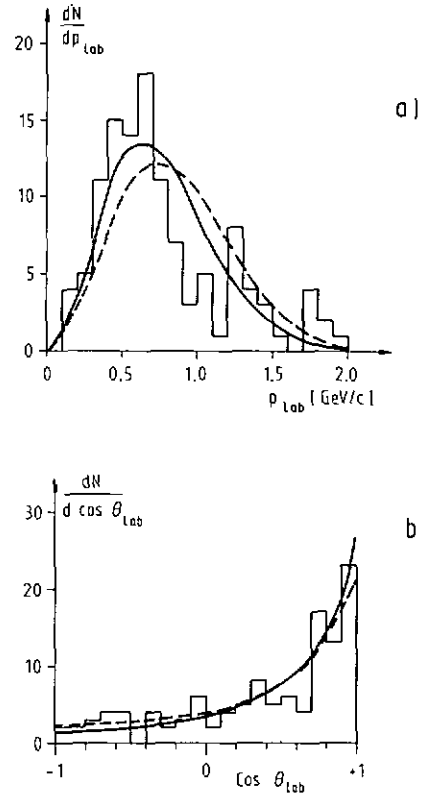

Fig. 16. DCE reaction: (a) momentum, (b) angular distributions for the three quickest protons. For explanation of curves, see fig. 15.

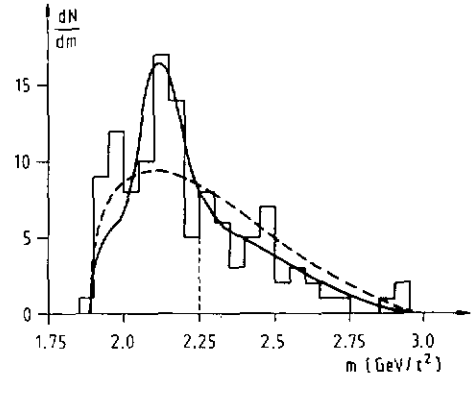

Fig. 17. DCE reaction. Proton–proton invariant mass distribution. For explanation of curves, see fig. 15.

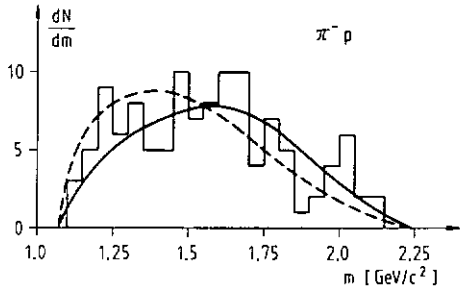

Fig. 18. DCE reaction. π^--proton invariant mass distribution. For explanation of curves, see fig. 15.

4.4. INTERPRETATION OF RESULTS

At high energies the models in subsect. 4.2 do not correctly reproduce the integrated cross section for DCE. Moreover, they all assume two spectator protons per event, whereas we observed an average of only 0.7 per event (see table 3).

These two observations lead us to interpret DCE as a 3-nucleon process. The simplest hypothesis involves a two-step reaction, as follows (see fig. 14d):

(i) production of one pion: $\pi^+ n \to \pi^+ \pi^- p$,

(ii) absorption of the π^+ by a p-n pair: $\pi^+(pn) \to pp$ (on-shell π^+ absorption is not possible kinematically on a single nucleon).

4.4.1. Integrated cross section calculation. The cross section was calculated using the following classical formula:

$$\sigma(\mathrm{DCE}) = 2\sigma_{\mathrm{He}}(\pi^+ n \to \pi^+ \pi^- p)\frac{1}{4\pi D^2}\int_0^\infty \sigma(\pi^+ d \to pp)\frac{dn}{dp}\,dp\,.$$

The use of $\sigma(\pi^+ d \to pp)$ for the absorption of a π^+ in ^{4}He is the delicate part of the hypothesis; it was shown in ref. [1]) that $\sigma(\pi^+(pn) \to pp)$ does not depend on isospin or spin of the nucleon pair, but one cannot exclude a dependence on the distance between the nucleons. Although this dependence is unknown, the parametrization given in ref. [31]) for $\pi^+ d \to pp$ was used. A review of the measurements is given in ref. [30]).

The constant D is the mean distance between a nucleon and a p-n pair. For this calculation the value $1/D^2 = 0.69\ \mathrm{fm}^{-2}$ was used [1]). dn/dp was defined as follows. The π^+ momentum spectra at 1.7 GeV/c were added, weighted by the measured cross sections (table 1), for the reactions π^+ ^{4}He$\to \pi^+\pi^-$3pn and π^+ ^{4}He$\to \pi^+\pi^-$2pd. For the reaction π^+ ^{4}He$\to \pi^+\pi^-$p ^{3}He the phase space distribution was used. The calculation of σ(DCE) using the phase space for the three reactions introduces a difference of 8% at 1.7 GeV/c (0.19 mb using the LIPS and 0.21 mb using the experimental sample). This small deviation permits the use of the phase

space distributions when $p_{beam} \neq 1.7$ GeV/c. The value of $\sigma_{He}(\pi^+ n \to \pi^+\pi^- p)$ is only known at 1.7 GeV/c, so it was assumed that the ratio $\sigma_{He}(\pi^+ n \to \pi^+\pi^- p)/\sigma(\pi^+ n_{free} \to \pi^+\pi^- p)$ is constant as a function of p_{beam}. The quantity $\sigma(\pi^+ n_{free} \to \pi^+\pi^- p)$ was determined by using the experimental values of the charge symmetry reaction $\pi^- p \to \pi^+\pi^- n$ [ref. [29])]. The resulting σ_{DCE} is given by curve (1) in fig. 13. The threshold for this reaction (in fact, the threshold for one-pion production) lies at $p_{beam} = 280$ MeV/c, but no extrapolation was done to that limit as the experimental cross section $\sigma(\pi^+ d \to pp)$ has large error bars at low energies [30]), and off-shell effects become important. The agreement with experiment at high energies is excellent but the measurement at 610 MeV/c is only partially explained.

4.4.2. Differential spectra. The π^- distributions are shown in fig. 15. Each event of the reaction $\pi^+ {}^4\text{He} \to \pi^+\pi^- 3pn$ has been weighted with the probability for the π^+ to be absorbed by a pn pair of the ^{4}He nucleus. The result (full curves of fig. 15) is quite satisfactory, since the excess of events at small angles is well accounted for.

The Fowl program [17]) does not permit the treatment of reactions where the number of particles varies. Therefore, the following technique was required to reproduce the differential spectra allowing for proton interference. Events of the type $\pi^4 + {}^4\text{He} \to \pi^- 3pp_s$ (see subsect. 4.3) were weighted by the probability that a pp pair is the result of a π^+ absorption. Then the π^- spectrum was weighted in a way to reproduce the above-mentioned distribution (fig. 15). This calculation reproduces the structure appearing in the p-p mass spectrum (fig. 17) which is a direct outcome of the absorption process $\pi^+ pn \to pp$. This result, in our opinion, seems to be the most significant for the validity of our interpretation. The $\pi^- p$ mass spectrum (fig. 18) also is correctly reproduced without the necessity of introducing baryonic resonances to explain the deviation from the phase space distribution. This weakens the validity of the interpretation given for our preliminary results [21]). The proton momentum distribution (fig. 16a) calculated with this model partially reproduces the extra protons present at low momentum. The residual excess of low momentum protons and the slight disagreement in the pp mass spectrum below 2.0 GeV/c^2 can be due to pp final-state interactions. They may also be consequences of some simplifications in the calculations.

The small number of events does not permit a test of the validity of our hypothesis using the χ^2 test. Nevertheless, the visual agreement between the experimental spectra and those resulting from our calculations seems to be sufficient to retain the interpretation we propose.

4.5. DISCUSSION

The cross section measurement of the double charge exchange reaction $\pi^+ {}^4\text{He} \to \pi^- 4p$ together with the study of the differential cross sections at 1.7 GeV/c have encouraged us to propose a new model for this reaction: production of one pion, followed by the absorption of the π^+ on a proton–neutron pair.

As a consequence of this model, one may infer the following:

(a) Over 280 MeV/c the double charge exchange is partially a 3-nucleon mechanism. Therefore, it is better to test the pair correlation models below this limit.

(b) The model proposed here liberates the Gibbs model [24]) from the constraint imposed by the measurement at 600 MeV/c [ref. [20])], thus reinforcing the position of this model.

(c) Our interpretation is in competition with the hypothesis of exchangc currents (see figs 14c, d). The first vertex of both the proposed mechanisms is the same, but at 1.7 GeV/c the proton–proton mass spectrum shows the dominance of diagram 14d. We deduce that, at least at high energies, the off-shell $\pi\pi$ effects are overestimated in the model used by Germond and Wilkin [27,28]). Experimental results between 0.6 and 1.0 GeV/c may give quantitative estimates of these effects.

We would like to thank our theorist colleagues Drs. C. Schmit and J.-F. Germond at Neuchâtel, together with Prof. C. Wilkin of the University College London, for helpful discussions. We are grateful to Dr. D. Roaf and his group, who built the Oxford/RHEL helium bubble chamber. Drs. M.G. Bowler in Oxford and J. Guy at RHEL provided us with the film, and we thank them warmly for their help. We appreciate the support we received at various stages of this experiment from our colleagues Dr L. Bachman, Dr. D. Perrin, and R. Schwarz. Finally, this study would not have been possible without the high quality work of our scanning and measuring team at Neuchâtel and the competence of the EPF-L computer centre at Lausanne.

References

1) J.-B. Jeanneret, Thesis, University of Neuchâtel (1978)
2) J.-B. Jeanneret, University of Neuchâtel, Institute of Physics, internal report (unpublished)
3) D. Roaf, C.A. Bailey, G. Davey, B.A. Hands, J. McKenzie, A.B. Miller, J. Moffatt, T.S. Peel, D.F. Shaw, W. Turner, G.C. Weeks, H. Hadley, M. Snowden, W.J. Tallis, R.N. Walker and W.T. Welford, Nucl. Instr. **64** (1968) 301
4) E. Wilkinson, Thesis, University of Oxford (1972)
5) Review of Particle Properties, Phys. Lett. **75B** (1978)
6) M.G. Bowler, private communication
7) CERN-Program Library, Documents X201 and X601
8) M. Bogdanski, J.-B. Jeanneret and E. Jeannet, Helv. Phys. Acta **51** (1978) 383
9) E. Fett, Herceg-Novi School (1966)
10) E. Lambert and H. Feshbach, Ann. of Phys. **76** (1973) 80
11) R.F. Frosch, J.S. McCarthy, R.F. Rand and M.R. Yearian, Phys. Rev. **160** (1967) 874
12) H. Uberall, in Electron scattering from complex nuclei (Academic Press, NY) p. 186
13) R.J. Mannings, Thesis, UCRL 19339
14) π^+p, π^+n and π^+d interaction – A Compilation, LBL-53 (1973)
15) J.-F. Germond, Thesis, University of Neuchâtel (1973)
16) G.R. Plattner and I. Sick, QED und der radius von ^{4}He, communication at the Swiss Physical Society (1978)
17) F. James, CERN-Program Library, CERN 68-15
18) M.M. Block, I. Kenyon, J. Keren, D. Koethke, P.K. Malhotra, P. Mazur, R. Walker and H. Weinzeler, Proc. Williamsburg Conf. on intermediate energy physics (1966)

19) I.V. Falomkin, V.I. Lyashenko, G.B. Pontecorvo, Yu.A. Shcherbakov, M. Albu, T. Angellescu, O. Balea, A. Mihul, F. Nichitin, A. Seraru, F. Balestra, R. Garfaghini, G. Piragino, C. Guaraldo and R. Scrimaglio, Nuovo Cim. Lett. **16** (1976) 525
20) N. Carayannopoulos, J. Head, N. Kwak, J. Manweiler and R. Stump, Phys. Rev. Lett. **20** (1968) 1215
21) F. Gaille, S. Mureramanzi, M. Bogdanski, J.-B. Jeanneret, E. Jeannet and D. Perrin, Nuovo Cim. **40A** (1977) 31
22) L. Gilly, M. Jean, R. Meunier, M. Spighel, J.P. Stroot and P. Duteil, Phys. Lett. **1** (1965) 335
23) L. Kaufman, V. Perez-Mendez and J. Sperinde, Phys. Rev. **175** (1968) 135
24) W.R. Gibbs, B.F. Gibson, A.T. Hess and G.J. Stephenson Jr., Phys. Rev. **C15** (1977) 1384
25) F. Becker and C. Schmit, Nucl. Phys. **B18** (1970) 607
26) J.-F. Germond, private communication (1978)
27) J.-F. Germond and C. Wilkin, Nuovo Cim. Lett. **13** (1975) 605
28) J.-F. Germond and C. Wilkin, in Mesons in nuclei, ed. M. Rho and D. Wilkinson (North-Holland, Amsterdam) ch. 4
29) $\Delta^{\mp}$, Compilation of cross-sections, CERN-HERA 72-1
30) C. Richard-Serre, W. Hirt, D.F. Measday, E.G. Michaelis, M.J.M. Saltmarsch and P. Skarek, Nucl. Phys. **B20** (1970) 413
31) B.S. Aladashvili, J.-F. Germond, V.V. Glagolev, M.W. Nioradze, T. Siemiarczuk, J. Stepaniak, V.N. Streltzov, C. Wilkin, P. Zielinski, J. Phys. **G3** (1977) 1225